Applied Thermal Engineering 279 (2025) 127640

Contents lists available at ScienceDirect

Applied Thermal Engineering

journal homepage: www.elsevier.com/locate/ate

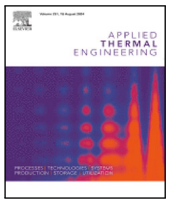

Research Paper

Comparison of oxygen carrier aided devolatilization behavior of wood pellets in a bubbling and spouted bed setup

Marian Schmitt *, Lennard Lindmüller, Alexander Fritzler, Stefan Heinrich

Institute of Solids Process Engineering and Particle Technology, Hamburg University of Technology (TUHH), Germany

ARTICLE INFO

Keywords:
Chemical looping
Oxygen carrier
Biomass conversion
Spouted bed
Devolatilization behavior

ABSTRACT

In the course of efforts to reduce emissions of carbon dioxide and to meet the global climate targets, the chemical looping combustion process (CLC) has increasingly received more attention over the years. In CLC the contact of the gasified solid fuel with the oxygen carrier is of great importance. Especially when combusting biomasses which include high amounts of volatiles, there is a risk of incomplete conversion of said volatiles. To tackle this challenge of volatile bypasses, the installation of a spouted bed is proposed to increase the mixing of solid fuel and oxygen carrier and thereby increase the conversion. Furthermore, the higher mechanical stress in a spouted bed can lead to fuel particle breakage which can result in higher fuel conversions. In this work biomass pellets were compared under spouted bed and bubbling bed conditions in a lab-scale hot plant. The influence of pellet size was studied and concentration profiles were tracked using online gas analytics. Stable operating conditions were found for the spouted bed setup and compared regarding conventional combustion and oxygen carrier aided devolatilization. Under spouted bed conditions higher carbon conversion, higher conversion rates and a higher degree of conversion were achieved. This increase was attributed to the better mixing and higher gas-solid contact in the spouted bed and the breakage of pellets and subsequent increase of specific surface area due to higher forces.

1. Introduction

In the human era, and especially since industrialization, there has been a significant acceleration of global warming processes due to human influence. One of the physico-chemical processes accelerating global warming is the greenhouse effect, which describes the rise in the surface temperature of a planet caused by the insulating properties of greenhouse gases due to their absorption of infrared radiation emitted by the planet. One of the main greenhouse gases is carbon dioxide (CO_2), which poses a huge risk for global warming due to the shear amounts, that are produced and emitted. The largest emitter of CO_2 (36 %) is the energy sector, i.e. the burning of coal, oil and natural gas to produce power and heat, with coal-fired power plants being the largest single source of CO_2 emissions globally [1].

One approach to addressing this problem involves carbon capture utilization and storage (CCUS) technologies, where CO_2 is captured, optionally purified, and subsequently utilized — for instance, in the chemical industry — or stored, such as in underground geological formations [2].

When renewable energy sources, such as biomass-based fuels, are used instead of fossil fuels in CCUS systems, the process is referred to as Bioenergy with Carbon Capture and Storage (BECCS). A significant advantage of this approach is the potential to achieve negative CO_2 emissions, considering that renewable biogenic materials have already absorbed and stored CO_2 from their environment during their growth. If the captured carbon is not released back into the atmosphere but rather utilized or stored, the process can be classified as net-negative in terms of emissions [3,4].

Another technology enabling CCUS is the chemical looping process. Chemical looping describes the process of moving an oxygen carrier material between two reactors to transport oxygen into a gasification or combustion process without the disadvantage of diluting the system with nitrogen from the air [5]. In most cases the chemical looping setup consists of two interconnected fluidized bed reactors, one of which acts as the air reactor and the other as the fuel reactor. In the air reactor, air oxidizes the oxygen carrier material and the partially used air is discharged. In the fuel reactor, a gasification agent (such as CO_2 or steam) and fuel (i.e., biomass) are introduced into contact with the oxidized carrier material. During this contact, the fuel is converted while the oxygen carrier is reduced. Nearly pure CO_2 gas is discharged at the end of the fuel reactor and can be further cleaned and purified for use in various CCUS technologies. Cyclones and loop seals

* Corresponding author.
E-mail address: marian.schmitt@tuhh.de (M. Schmitt).

https://doi.org/10.1016/j.applthermaleng.2025.127640
Received 30 March 2025; Received in revised form 11 June 2025; Accepted 20 July 2025
Available online 29 July 2025

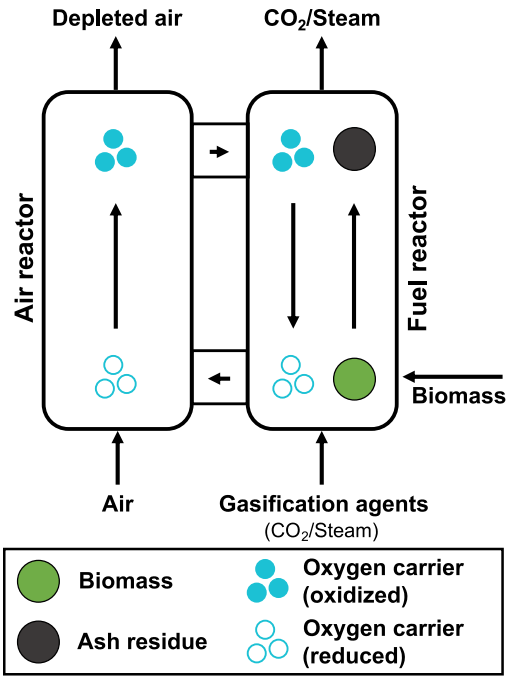

Fig. 1. Schematic of chemical looping process under iG-CLC conditions using biomass as solid feedstock.

connect the two reactors to prevent mixing of the different gas phases. Oxygen carrier particles are alternately reduced in the fuel reactor and oxidized in the air reactor in a circular looping process [6]. A graphical visualization of the CLC process is shown in Fig. 1.

Over 50 pilot plants are operated globally following the CLC principle, most of them using gaseous fuels like syngas or methane [7] or solid feedstock like coal [8] or biomass [9]. Different reaction routes can be realized, which can be grouped into two main process conditions: In syngas-CLC, the solid fuel undergoes gasification in a preliminary step before being introduced into the process. Alternatively, in in-situ gasification CLC (iG-CLC), the fuel is gasified directly within the process itself. The reaction pathway of iG-CLC is illustrated in Fig. 2. In this process, the fuel first undergoes drying and devolatilization, during which the released volatile compounds can react with the oxygen carrier. The resulting gas products, in combination with the fluidization gas composed of the gasification agent, enables the gasification of the remaining char, consisting of fixed carbon and ash. In actual plant operation, devolatilization and gasification occur simultaneously.

Using Biomass as solid fuel in CLC poses additional challenges to the ones, solid feedstock poses anyways. In addition to the dangers of mineral content in biomass ash, that can lead to agglomeration, sintering and subsequent defluidization of the bed, the high volatile content of biomass and quick devolatilization can lead to gas bypasses in the bed and therefore lower gas-solid contact between volatiles and bed material. This effect is even more dramatic for large particles, as these particles tend to swim on top of the bed, where the released volatiles do not have the chance to get in contact with the bed material.

Different approaches are found in literature to tackle the lower gas contact and the arising problems. Using a oxygen carrier material with oxygen uncoupling properties (CLOU) could be one solution, as these materials release gaseous oxygen at high temperatures and therefore enable gas-gas contact even above the bed and increase volatile conversion by that [10]. To increase the residency times of volatile matter a pilot plant featuring a two-stage fuel reactor design, where unreacted volatiles will have the chance to be further converted in the upper stage, was proposed by Thon et al. [11] and built at TUHH. The use of biomass as solid feedstock was studies in depth by Haus et al. [12] and Lindmüller et al. [13,14]. The drawback of a two-stage design however is its higher pressure drop compared to a one-stage reactor and its difficulty in upscaling. An alternative option to increase gas-solid contact is the implementation of a spouted bed instead of a bubbling bed. In spouted beds, the fluidization gas is not fed over the entire cross-sectional area of the bed, but only through a gap or nozzle. This creates a fountain in the center of the bed in which the particles are accelerated upward and then fall back down the reactor wall. Due to this back-mixing, spouted beds generally exhibit higher heat and mass transfer, which strongly favors sterically hindered chemical reactions [15]. Spouted beds also tend to have lower pressure drops over the bed height, which would be beneficial for upscaling processes because less energy would be required for fluidization.

Spouted bed technology is seldom applied in Chemical Looping Combustion (CLC), with only a few facilities implementing this design. A notable aspect of these approaches is the use of spout-fluid beds, where the central gas inlet is supported by a lower-volume gas flow in the surrounding region. Compared to other reactor configurations, the spout fluidized bed achieves a more uniform temperature distribution, slightly improved combustion efficiency at lower bed temperatures, and a higher heat transfer coefficient between the bed and its surface [16]. Research on combustion processes in spout fluidized bed reactors has largely been conducted in pilot-scale setups, with variations in both fuel type and reactor design. These studies consistently employed reactors featuring either a rectangular or circular conical lower section with inclination angles between 28° and 60°. A comparative evaluation of different nozzle types such as round, slot, and annular slot, indicated that slot nozzles produced the highest CO concentrations, suggesting inefficient combustion. This inefficiency is likely due to the inability to establish a stable operating range for the slot nozzle at the given air flow rates. In contrast, the annular slot nozzle demonstrated the highest combustion efficiency, along with slightly better carbon conversion and gasification performance during charcoal gasification [17,18]. Overall, the findings indicate that this technology is sufficiently developed for large-scale industrial application. However, a significant challenge remains in optimizing the reactor's design and scaling it appropriately, because the stable operation regime is more limited in comparison to bubbling bed reactors [19].

One of the challenges associated with spouted bed reactors however — particularly in the context of scale-up and large-scale applications — is the attrition of bed material [20]. In general, attrition rates in spouted beds tend to be higher than those in fluidized beds [21]; however, the actual extent of attrition depends significantly on the operating mode, reactor design, and process conditions. Under favorable conditions, it is possible to minimize attrition even in spouted bed systems. For instance, the incorporation of draft tubes has been shown to reduce particle attrition, and the same study also reported a correlation between attrition rates and fluidization velocity [22]. It is important to note, however, that bed material attrition is not limited to the fuel reactor in CLC or circulating fluidized bed (CFB) systems. Significant wear also occurs in cyclones, the upper sections of risers, and in bends and pipelines throughout the system. Therefore, attrition observed in the fuel reactor represents only a fraction of the total material degradation in such processes.

This work will focus on the improvement of the reaction between bed material and released volatiles (gas-solid contact) and the interaction between pellets and the bed (solid-solid contact) by introducing a spouted bed reactor setup with similar general dimensions as the bubbling bed version, to ensure the capability to perform direct comparison between the fluidization regimes. Spouted bed conditions are ensured by performing in-depth stability analysis by studying the frequency distribution of pressure differences in the reactor. The first step was to study conventional combustion using air as fluidization medium and inert sand as bed material. To take an intensive look into the devolatilization behavior of woody biomass pellets, in the second step, oxygen carrier was used as bed material and nitrogen was chosen as fluidization gas for devolatilization experiments to specifically bring gasification reactions with CO_2 or steam to a minimum.

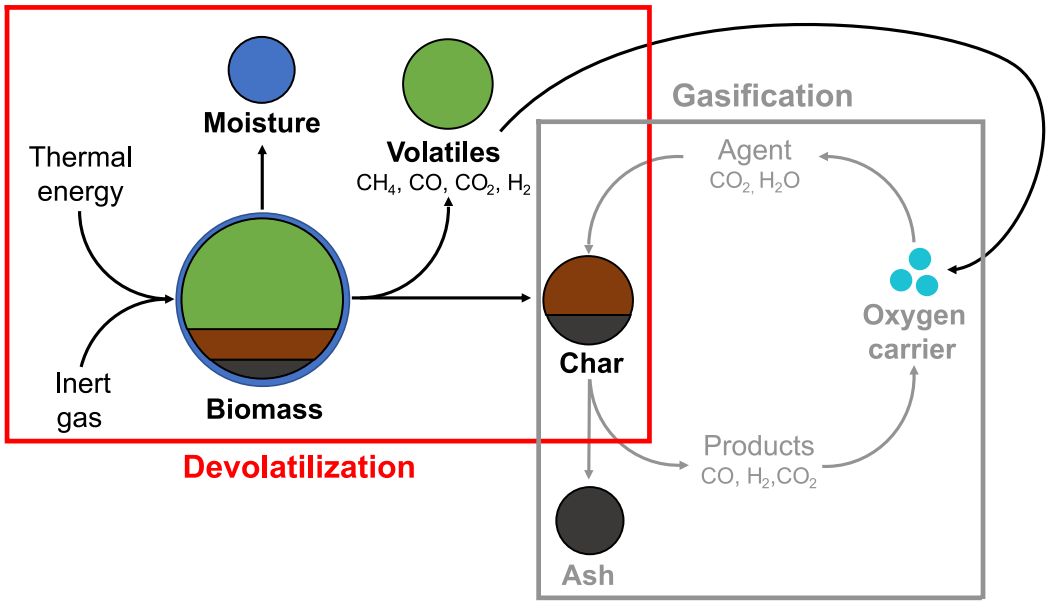

Fig. 2. Visualization of the reaction mechanism of the whole iG-CLC process with marked sections for the devolatilization and gasification part to highlight the process that was investigated in this study.

2. Experimental setup

2.1. Lab-scale plant

To study the devolatilization in a controllable environment, suitable conditions were produced in the lab-scale hot fluidized bed, shown in Fig. 3. The plant consists of a chrome-nickel-steel tube, that is 53 mm in diameter with a length of 650 mm. Using two PID controllers, a 4 kW electrical heating unit can heat the plant up to 1100 °C. Fluidization gases are pre-heated in a coiled pipe before entering the reactor through a gas distributor made from sintered metal. To control the process, temperatures are measured at different points in the reactor, namely below and above the gas distributor, in the freeboard phase of the reactor and in the gas outlet stream. Pressures are also measured between these points as pressure differences and additionally a total pressure inside the reactor is measured in comparison towards the atmosphere. Solenoid valves are used to switch the inflow between reducing, oxidizing and inert gases. Rotameters are used to control the volumetric flow rates of the singular gases.

2.2. Spouted bed design

The design of the spouted bed plant was based on previous investigations of spouted bed setups and the resulting empirical equations, and is shown in Fig. 4.

Prior to this, measurements of the pressure drop across the nozzle with different gas inlet openings as a function of the volume flow were carried out in a cold system. The spouting behavior and stability was also investigated visually in systems with conical and pyramid-shaped lower sections. Cold models of different nozzles were tested extensively with 3D printed parts and connecting them to a rectangular cuboid made of acrylic glass. The purpose of this was not only to study the existence and stability of the spout, but also to determine whether and to what extent bed material falls into the gas inlet after stopping the gas flow. To minimize the material loss, another nozzle was placed in a mirror-symmetrical arrangement just before the gas inlet opening, making the whole inlet design similar to a Laval-nozzle. Additionally, the gas inlet-pipe was bent by 180° to prevent solids from penetrating deeper into the piping system. When the system is restarted, the bed material in the inlet pipe is transported back with the gas flow. The inner diameter of the pipe and Sauter mean diameter of the bed materials were used for the empirical correlations to design the spouted bed. The diameter of the nozzle D_0 was set to 2.5 mm in accordance with Eq. (1) in order to achieve an ratio between nozzle diameter and particle diameter of 6.3 for sand and 9.1 for oxygen carrier [24,25]:

$$\frac{D_0}{d_{Sa}} = 2...20 \tag{1}$$

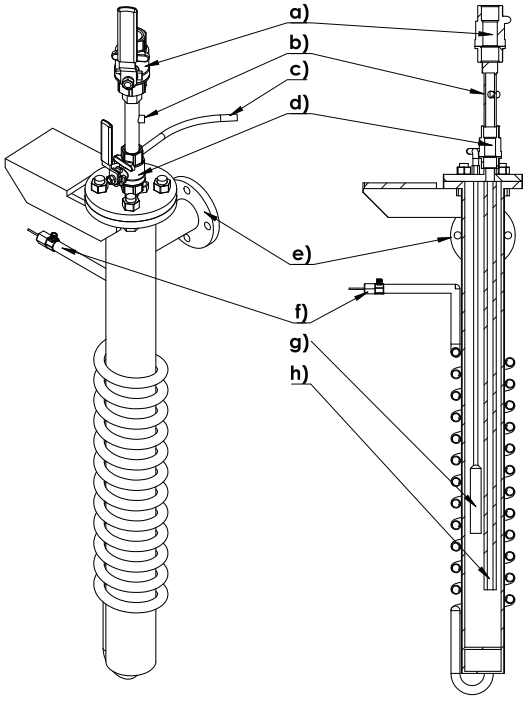

Fig. 3. Exterior and sectional view of the bubbling bed lab-scale hot plant (d_i = 53 mm, h = 650 mm) with measurements in mm. (a) and (d) ball valves used as solid feeding sluice (b) N_2 purge stream inlet (c) sample gas line for analytic (e) exhaust gas outlet (f) fluidization gas inlet (g) sample gas filter (h) above-bed style feeder.
Source: Modified from [23].

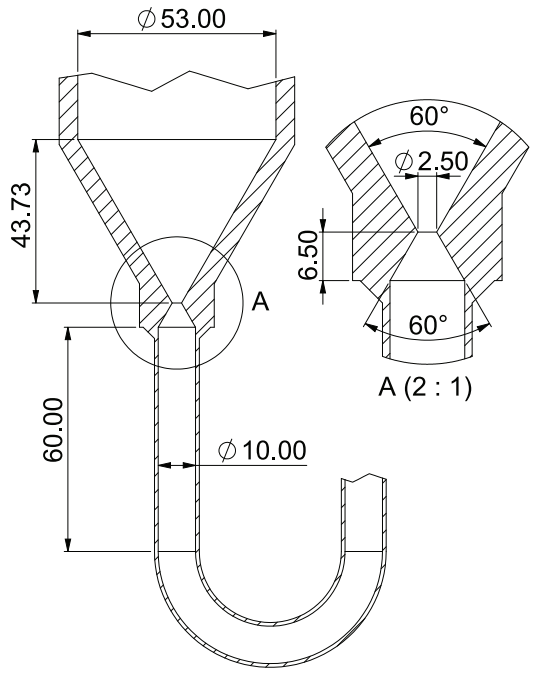

Fig. 4. Detailed view of the conical part of the spouted bed setup with measurements given in mm and zoom on the used Laval-like nozzle.

The length of the stabilization zone before the nozzle H_{in} is at 60 mm according to Eq. (2) to reach 4.8 times its minimal length $H_{in,min}$ in order to achieve a developed flow and largely minimize turbulent effects, to achieve stable spouting conditions:

$$H_{in,min} = 5 \cdot D_0 \tag{2}$$

The lower conical part has an angle of $\gamma = 60°$ and a cone height of 43.7 mm down to the nozzle opening according to Epstein et al. [26].

2.3. Online gas analytic

The exhaust gas first passes a ceramic filter (Fig. 3g). It then passes a filter consisting of a glass filled with filter wadding to separate coarse particles and an air filter with a hydrophobic PTFE membrane with a pore size of 0.2 µm to separate fine particles. The gas then passes a sample gas conditioner to remove moisture by cooling it to a dew point temperature of approx. 2–3 °C. The dry and cooled exhaust gas flow is then passed through an inline adsorber filter series circuit consisting of two adsorption filter units for removing nitrogen oxides and a filter unit for separating fine particles (<0.1 µm). The downstream vacuum pump conveys the exhaust gas further through a universal filter to remove the remaining solid impurities before the exhaust gas is fed to the exhaust gas analysis modules. At this point, part of the volume flow is passed through a stationary process gas analyzer. This consists of four individual modules connected in series in the following order, where the volume concentrations of the exhaust gas components, such as methane, carbon monoxide, carbon dioxide and hydrogen, are measured. CO_2 (0–100 vol.%), CO (0–25 vol.%) and CH_4 (0–45 vol.%) are measured non dispersive using infrared sensors (NDIR). H_2 (0–25 vol.%) is quantified with a thermal conductivity detector using values of the other modules to correct for the change in thermal conductivity. The fabricator is TAD GmbH in Unna, Germany (type GME.84-K4). The other part of the gas flow is passed though a oxygen-analyzer (MAGNOS 3K from H&B) that measures the oxygen concentration on basis of the paramagnetic properties of oxygen in the range of 0–30 vol.%. The entire structure of the system, including the exhaust gas conditioning and the analyzers used, is shown in Fig. 5.

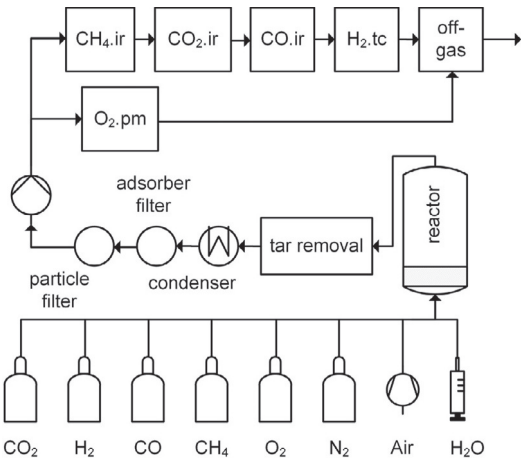

Fig. 5. Flowsheet of the reactor system including exhaust gas treatment and analyzers. *Source:* Modified from [23].

2.4. Solid feeding system

Pellets are fed into the reactor chamber during operation via a solids sluice. This consists of a long plastic tube that connects directly to the flange connection at one end. A funnel is fitted at the top to ensure that the solids are effectively fed into the system. Gases are initially prevented from escaping from the reactor by two threaded clamps. These are opened and closed in sequence to feed the fuel safely and precisely into the system. Cooling fins at one end, where the solids lock comes into contact with the flange connection, dissipate excess heat, preventing carbonization and plastic deformation of the plastic tube, the pellets are fed through. At higher temperatures (> 800 °C), it is possible to connect a nitrogen bottle via a three-way connector to make the cooling of the solids lock more effective. The above-bed feeding method is used in both systems. The wood pellets are introduced above the fixed bed mass in order not to disturb the fountain formed in the blast layer and to create the same conditions.

2.5. Experimental plan

For both combinations of bed material and fluidization gas, an in-depth stability analysis was conducted on the basis of both optical assessment as well as frequency analysis of the pressure signal. First, spouted bed and bubbling bed were compared for conventional biomass pellet combustion, by fluidizing 49 g of quartz sand with air with 8.05 l/min. Then, oxygen carrier aided devolatilization was conducted in both reactor types by fluidizing 34.4 g of oxygen carrier particles with nitrogen with 3.6 l/min. Both of these bed material masses result in a bed volume of 33 cm^3. For each of these 4 cases, 6 pellet masses between 0.9 and 1.4 g were investigated. The tests were carried out at 800 °C and in duplicate in each case, resulting in a total number of 48 experimental runs.

3. Materials and methods

3.1. Biomass

As biomass, whole wood pellets by PowerPellets Vertriebs GmbH & Co. KG (Germany) were used. There diameter was kept the same during the experiments, but their length was varied to match a certain mass. The Ultimate Analysis (NCHS analysis) was conducted in a Vario Macro Cube by the central laboratory of the TUHH to determine the elemental composition of the raw material in regards to nitrogen (N), carbon (C), hydrogen (H) and sulfur (S), where the rest of the elemental composition is assumed to be oxygen (O), so it gets calculated by

Table 1
Proximate and ultimate analysis of raw biomass pellets.

Proximate analysis		
Moisture	wt.% (raw)	8.1
Volatiles	wt.% (raw)	76.6
Ash	wt.% (raw)	0.1
Fixed Carbon	wt.% (raw)	15.1
Ultimate analysis		
N	wt.% (raw)	< 0.1
C	wt.% (raw)	47
H	wt.% (raw)	6.5
S	wt.% (raw)	< 0.2
O	wt.% (raw)	38.4

Table 2
Bed material properties of inert sand and oxygen carrier (OC).

Bed material properties			OC	Sand
Apparent density	ρ_s	[kg/m^3]	3858.1	2648.9
Sauter mean diameter	d_{sa}	[µm]	276.6	400.1
Porosity	ϵ	[–]	0.74	0.44
Bulk density	ρ_{bulk}	[kg/m^3]	1043.8	1487.5
Bed volume	V_{bed}	[cm^3]	33	33
Minimal fluidization velocity	u_{mf}	[m/s]	2.3	5.7
Oxygen transport capacity	R_O	[wt.%]	1.976	–

subtraction of sum of the other amounts. The results are shown in Table 1. Furthermore, a proximate analysis was conducted according to DIN 51718 [27], DIN 51719 [28] and DIN 51720 [29]. A more extensive analysis on the pellet properties used in this work can be found in Sadeq et al. [30].

3.2. Bed material

In the case of a classic combustion using air, an inert bed material in the form of quartz sand is used to not disturb the gaseous reactions. During the study of the chemical looping conditions inside the different reaction chambers, an oxygen carrier material is used. This oxygen carrier consists of γ-alumina particles impregnated with copper nitrate to form Cu-O on the surface. The manufacturing process was introduced by de Diego et al. [31] and a deeper insight into the restructuring of the copper to $CuAl_2O_4$ is given in Lindmüller et al. [13]. In this work it is also described, that the initial CLOU properties of the oxygen carrier faded, due to the restructuring of the copper into $CuAl_2O_4$, which is described in depth by Bolt et al. [32]. Although the copper aluminate spinel generally exhibits lower reactivity compared to copper oxide, the oxygen carrier used in this study has already undergone over 100 h of operation in a pilot plant. As a result, it has reached a stable state beyond the initial degradation phase, ensuring a consistent oxygen transport capacity (R_O). During the degradation process, R_O decreased from 2.5 wt.% to the listed 1.97 wt.%, accompanied by a loss of oxygen uncoupling (CLOU) activity. The use of this stabilized material provides a reproducible basis for the experiments.

The most important properties of both bed materials are shown in Table 2.

The bulk density was determined by calculating the ratio between the mass of the bed material m_{tot} and the volume it occupied within a cylindrical vessel of known volume V_{bulk} following Eq. (3):

$$\rho_{bulk} = \frac{m_{tot}}{V_{bulk}} \tag{3}$$

Apparent density ρ_s is measured via gas pycnometer (Multivolume Pycnometer 1305 from MICROMETRICS) using helium as the test gas.

The porosity of the bed materials is calculated with Eq. (5) based on the assumption that the bulk porosity $\epsilon_{bulk} = 0.4$ and the total porosity ϵ_{tot} is calculated following Eq. (4):

$$\epsilon_{tot} = 1 - \frac{m_{tot}}{\rho} \tag{4}$$

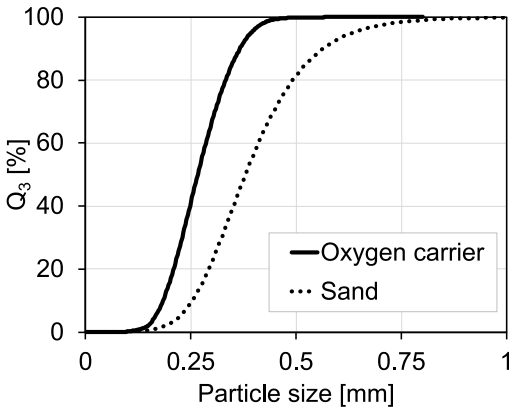

Fig. 6. Cumulative mass-based particle size distribution of bed materials.

$$\epsilon = 1 - \frac{1 - \epsilon_{tot}}{1 - \epsilon_{bulk}} \tag{5}$$

R_O is calculated by comparing the mass of fully oxidized oxygen carrier $m_{OC,ox}$ to the mass of fully reduced oxygen carrier $m_{OC,red}$ following Eq. (6). For that, the material is first fully reduced using the described pilot plant and methane as reductive gas. Afterwards, it is oxidized using a muffle furnace:

$$R_O = \frac{m_{OC,ox} - m_{OC,red}}{m_{OC,red}} \tag{6}$$

The minimal fluidization velocity shown is the value for 800 °C obtained from the Ergun equation (7) and (8), after validating the usability of said formula using measurements at ambient conditions:

$$\frac{\Delta p}{H_{bed}} = 150 \cdot \frac{(1-\epsilon)^2}{\epsilon^3} \cdot \frac{\eta_f \cdot u}{d_{Sa}^2 \cdot \psi_{Wa}^2} + 1.75 \cdot \frac{1-\epsilon}{\epsilon^3} \cdot \frac{\rho_f \cdot u^2}{d_{Sa} \cdot \psi_{Wa}} \tag{7}$$

$$\Delta p = (1-\epsilon) \cdot (\rho_s - \rho_f) \cdot g \cdot H_{bed} \tag{8}$$

This minimal fluidization velocity applies to the operation of the bubbling bed reactor and cannot be applied to the spouted bed setup. Stable operation points for the spouted bed were found using the Fast-Fourier transformation. See Section 3.4 for a more thorough explanation.

Particle size distributions of the two bed materials were measured using a CAMSIZER XT from Retsch Technology. The measurement is based on a dynamic image analysis and the detected area of particles was used for the evaluation of the particle size distribution. The cumulative mass-based particle size distribution of both bed materials is shown in Fig. 6. The Sauter mean diameter was calculated based on these measurements.

3.3. Data evaluation

To determine the process in both the bubbling bed and the spouted bed setup and compare them, a set of key parameters need to be introduced. The first way to determine the process differences between the two setups, is a comparison of the analyzed gas concentrations of all relevant gases.

The carbon conversion X_C indicates how well the supplied solid carbon is converted over the process time. It is determined from the ratio of the total amount of carbon detected in the exhaust gas $m_{C,out}$, and the total amount of carbon in the fuel $m_{C,tot}$, that is determined by the mass of the biomass and the ultimate analysis of said material according to Eq. (9):

$$X_C = \frac{m_{C,out}}{m_{C,tot}} \tag{9}$$

where the mass of all carbonaceous gases at a given process time $m_C(t)$ is determined by Eq. (10):

$$m_C(t) = \frac{p_{out} \cdot M_C}{R_{uni} \cdot T_{out}} \int_0^t F_{out} \cdot Y_{C,out}(t) - F_{in} \cdot Y_{C,in}(t) \quad (10)$$

The pressure inside the analyzer p_{out} is assumed to be atmospheric and the temperature inside the cabinet T_{out} is monitored during the experiments. The molar mass of carbon M_C and the universal gas constant R_{uni} are taken from literature. The in-going volumetric flow F_{in} is measured at all times and is the sum of the fluidization gas and the purge gas used in the solid feeding system, with $Y_{C,in}$ being the molar fraction of carbon in said flow. The outgoing volumetric flow F_{out} is determined by using the concentration of nitrogen Y_{N_2} according to Eq. (11), because the amount of nitrogen in the biomass is determined to be negligible small and nitrogen as inert gas will not partake in any chemical reactions, so it can be assumed, that the total volumetric flow of nitrogen F_{N_2} stays constant between in-stream and out-stream of the reactor unit:

$$F_{out} = \frac{F_{N_2}}{Y_{N_2}} \quad (11)$$

The concentration of nitrogen in the flue gas is determined by difference from the other measured gases.

During the devolatilization of the biomass inside the reactor, the volatiles will react with the oxygen from the air or the oxygen carrier material respectively, to get oxidized up to the final oxidation stage (CO_2 and H_2O). To determine how well the volatiles react to carbon dioxide, the fraction of the molar fraction of carbon dioxide Y_{CO_2} on the summed up molar fraction of all carbonaceous gases is defined as the carbon dioxide specific degree of conversion $\eta_{CO_2,conv}$ according to Eq. (12):

$$\eta_{CO_2,conv} = \frac{Y_{CO_2}}{Y_{CH_4} + Y_{CO} + Y_{CO_2}} \quad (12)$$

3.4. Stability analysis of spouted bed

Because a visual determination of a stable working range is not feasible in a fully isolated hot plant, the stability of the spout has to be determined non-optically. To realize this, a stability analysis was carried out using the Fast Fourier Transformation (FFT) according to Eq. (13):

$$F(k) = \sum_{j=1}^{N} x(j) e^{-i\frac{2\pi}{N}(j-1)(k-1)} \quad (13)$$

For this purpose, a high-frequency pressure sensor was used to record the total relative pressure of the system compared to its atmosphere at different fluidization gas streams and operating temperatures. Using the FFT, this pressure fluctuation signal can be transferred to the frequency domain and the peak distribution can be used to make a statement about the stability of the spout. By using low-pass and high-pass filters, peaks in the low frequency range (<5 Hz) can be eliminated, as these are only predominantly caused by particle movements in the fixed bed. In the case of a stable operating point, a clear single dominant peak can be recognized in the range of 5–15 Hz, as fluctuations of the pressure difference in this frequency range are caused by particle movements in the fountain [33]. Peaks in higher frequency ranges tend to stem from movements of single particles or small particle clusters in the freeboard phase above the bed and spout region and signal a instability of the spout due to too high fluidization velocities.

4. Results

4.1. Stability analysis

In addition to experiments on the cold plant, in which the cylindrical part of the system was replaced by Plexiglas in order to be able to qualitatively evaluate the spouting behavior optically, a stability analysis based on the Fast Fourier Transformation was also carried out. For that, the relative pressure of the plant was measured against the atmosphere with a high frequency of 2.5 kHz, while the spouted bed was at operating temperature of 800 °C. The pressure signal was then transposed into the frequency domain as shown in previous chapters. Because the stability of the spout is not only a function of the volumetric flow rate, but also of properties of the bed and material and fluidization gas, a stability analysis was carried out for both configurations studied in this work — quartz sand with air and oxygen carrier with nitrogen. Fig. 7 shows the pressure signal recorded at 2.5 kHz on the left and the corresponding representation in the frequency range after the FFT has been carried out on the right.

These stability analyzes were carried out at 4 different temperatures (20 °C, 200 °C, 500 °C, 800 °C) and at 14 different gas volume streams ranging from 4.3 to 43 l/min for air and 10 different gas volume streams ranging from 1.75 to 12.5 l/min for nitrogen. The evaluation of these conditions resulted in choosing the following operating conditions: 8.05 l/min of air for fluidization of sand and 3.6 l/min of nitrogen for fluidization of oxygen carrier. This corresponds to gas velocities of 6.1 cm/s and 4.2 cm/s respectively, which results in fluidization numbers of 1.1 for combustion and 1.8 for the devolatilization. Under these conditions a stable spout in the spouted bed reactor and bubbling conditions in the bubbling bed reactor can be ensured.

4.2. Combustion

After finding stable operation points for the spouted bed, the first comparison between reactor types was conventional combustion of wood pellets using sand as inert bed material and air as fluidization gas. This allowed for an evaluation of the differences in gas-gas contact, as this type of contact is the most dominant in combustion with air. The composition of exhaust gases during the combustion process with air is illustrated as an example for a pellet mass of 1.4 g, comparing the two reactor types in Fig. 8. Quartz sand was utilized as the bed material, and an air flow rate of 8.05 l/min was set. In this case the combustion process took 390 s in the bubbling bed and 420 s in the spouted bed. As expected, lower pellet masses resulted in decreased conversion times, reaching 360 s in the bubbling bed and 390 s in the spouted bed for the combustion of 0.9 g.

At the lowest pellet mass of 0.9 g, the oxygen concentration drops to 5.5 vol.% in the bubbling bed and 4.8 vol.% in the spouted bed as shown in Fig. 9. At a pellet mass of 1.4 g, however, the O_2 concentration temporarily drops to 0 vol.%, indicating that only sub-stoichiometric combustion can occur in the surrounding period. This results in elevated concentrations of carbon monoxide (CO) in the exhaust gas, as shown in Fig. 8. The non-conversion of methane (CH_4) is visible through a peak of methane at around 0.3 vol.% for the spouted bed, whereas no amount was detectable in the bubbling bed setup. Hydrogen trends were not distinguishable between reactor types and peaked around 0.55 vol.%. Methane was only detected in the spouted bed setup with high pellet masses, again demonstrating the sub-stoichiometric conditions present, during complete oxygen depletion. In the case of 1.4 g CH_4 concentrations of up to 0.35 vol.% were detected.

Additionally, the pyrolysis-like state leads to the production of tars and other long-chain hydrocarbons, which are not captured by the online measurement analysis utilized and thus are not considered in the carbon balance. This tar formation is especially prominent with partially devolatilized particles floating on the bed surface [34]. Mendiara et al. [9] studied tar formation under iG-CLC conditions in detail.

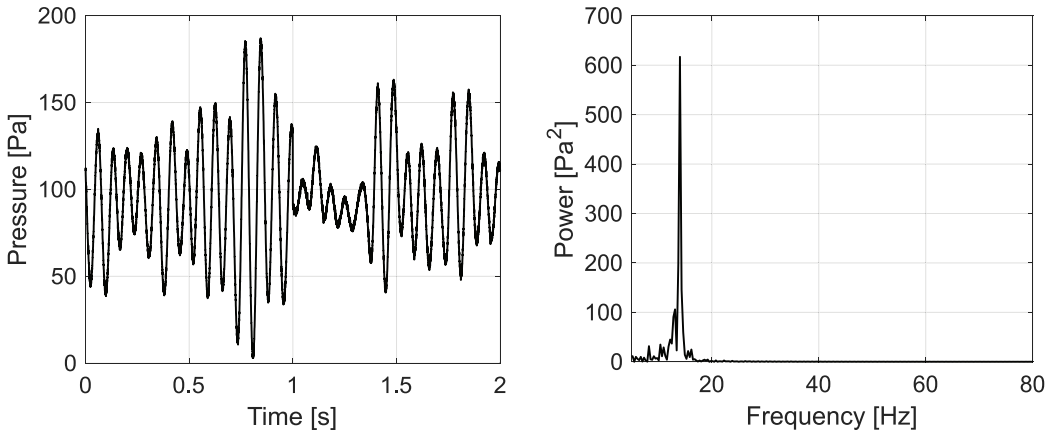

Fig. 7. Total relative pressure signal against atmosphere over time (left) and transformed signal using FFT (right) for quartz sand at 800 °C and air fluidization at 8.05 l/min.

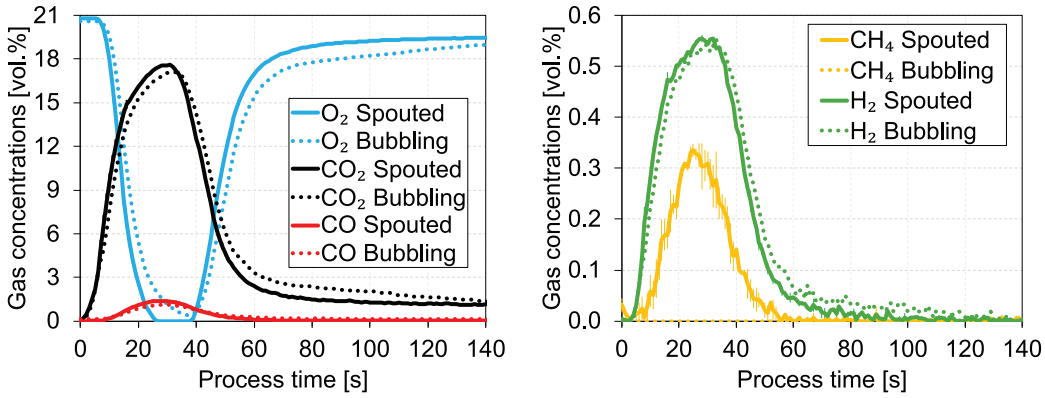

Fig. 8. Average dry gas concentrations of CO_2 and CO during two combustion experiments at 800 °C under bubbling and spouted bed conditions of 1.4 g of biomass using inert sand as bed material and air as fluidization gas with 8.05 l/min.

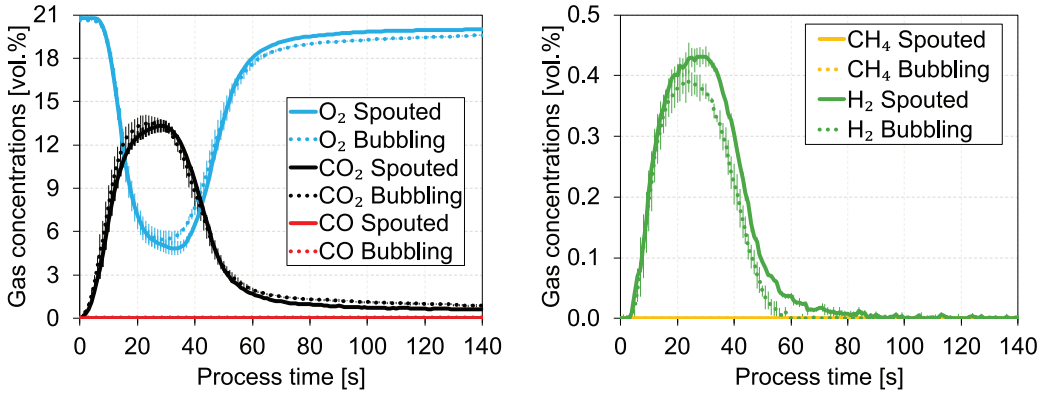

Fig. 9. Average dry gas concentrations of CO_2 and CO during two combustion experiments at 800 °C under bubbling and spouted bed conditions of 0.9 g of biomass using inert sand as bed material and air as fluidization gas with 8.05 l/min.

Under comparable conditions to this work (fuel reactor temperatures of 900 °C, Fe-based oxygen carrier and pine saw dust as biomass) they detected between 1.59 to 2.76 g/kg$_{fuel}$ of tar. These amounts of tar formation would result in an error in the carbon balance below 1 %. It should be noted, that under lower reaction temperatures more tars seem to form [35], but the iron-based oxygen carrier used generally shows lower reactivity compared to the Cu-based oxygen carrier used in this study [36]. Based on these considerations, it is reasonable to assume that the carbon balance is not significantly affected by not considering tar formation.

Any comparison of total carbon conversion, conversion rate and process time are therefore not representing the actual kinetics of the process, as with oxygen concentration reaching zero, sub-stoichiometric reactions occur. The fact that more oxygen is needed during the pellet combustion in the spouted bed system is attributable to wood pellet fragmentation and abrasion, which is induced by the increased forces acting on the fuel in the spouted bed from the bed material. The pellet fragmentation results in an increase in the specific surface area and, consequently, higher particle-particle contact and enhanced kinetics. Additionally, enhanced gas-solid contact resulting in forced convection accelerates the combustion and therefore depletes the air of oxygen.

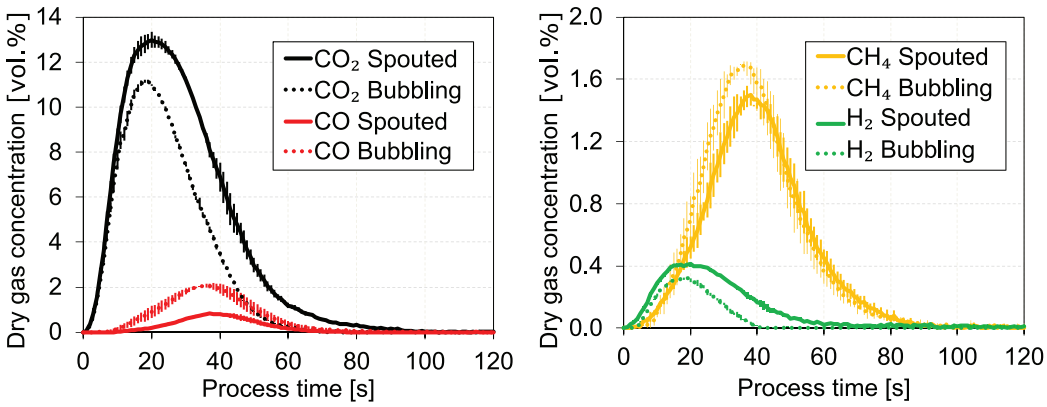

Fig. 10. Average dry gas concentrations of CO_2 and CO (left) and dry gas concentration of CH_4 and H_2 (right) using oxygen carrier as bed material, nitrogen as fluidization gas with 3.6 l/min and a pellet mass of 0.9 g.

The pellet fragmentation was qualitatively verified through experiments conducted in a cold plant using degassed char pellets, where the breakage of the pellets occurred more rapidly in accordance with the devolatilization state of the material.

4.3. Oxygen carrier aided devolatilization

To assess the influence on the solid-gas contact in either bubbling or spouting conditions, experiments were conducted for oxygen carrier aided devolatilization. The listed case examples are given for a pellet mass of 0.9 g. The experiments were carried out with a nitrogen flow rate of 3.6 l/min.

Since the conversion of gases during this process can only occur via solid-gas contact, rather than gas-gas contact as in combustion, the interaction between devolatilized gases and the bed material is of central importance. In a bubbling bed, the large size difference between the pellets and the bed material as well as the degassing of wood pellets during fluidization causes the pellets to float on the bed surface [37,38]. When devolatilization occurs in this region, the contact between the released gases and the bed material is significantly limited. As a result, the gases are only partially or insufficiently converted by the oxygen carrier and exit the reactor unconverted. In contrast, in a spouted bed, the improved mixing of the pellets with the bed material through their consecutive upwards motion in the radial center and downwards motion at the wall region, allows devolatilization to occur even in the lower region of the bed. Therefore, the gases generated by devolatilization have a significantly higher contact with the bed material. This means, that even though the mean residence time of fluidization gases is the same for both setups, the residence time distribution of the released gases is broader and higher on average in the spouted bed compared to the bubbling bed. This broadening primarily occurs towards longer residence times due to degassing in the lower bed zones. However, the higher gas velocities in the reactor's core can also lead to the premature ejection of unconverted gases when degassing occurs in the upper spout region. This superimposition of the residence time of the gases with the position distribution of the devolatilizing pellet leads to better conversion in the spouted bed. These differences can be observed in all the effects discussed below.

4.3.1. Process time

Fig. 10 shows a process time of around 90 s in the bubbling and 100–110 s in the spouted bed. In this figure, all data points represent duplicate measurements, and error bars are visualized. As with the combustion with air described in the previous chapter, the longer process time results from the overall higher carbon conversion. This increase in conversion also occurs during devolatilization due to the breaking up of the pellets and the associated increase of the specific surface area. The increase in process times is not indicative of worse conversion performance but rather a result of improved mixing. As total carbon conversion increases, a longer process time should not be interpreted as a negative outcome. Generally, the process occurs at a faster rate than combustion because devolatilization proceeds more rapidly than the gasification sub-process, and with an even greater rate than coke combustion. In the example case shown in Fig. 10, it is evident that the concentrations differ between the two reactor types. Specifically, the spouted bed exhibits consistently higher CO_2 and lower CO levels compared to the fluidized bed. This suggests a more efficient and complete conversion in the spouted bed. These differences are systematic and persist across all studied pellet sized. In contrast, variations in methane and hydrogen concentrations do not appear to follow a consistent pattern and are generally less pronounced. The following chapter will provide a more detailed analysis of the absolute molar quantities of the individual gas components derived from the concentration profiles, enabling a systematic rather than merely symptomatic comparison of the two reactor types.

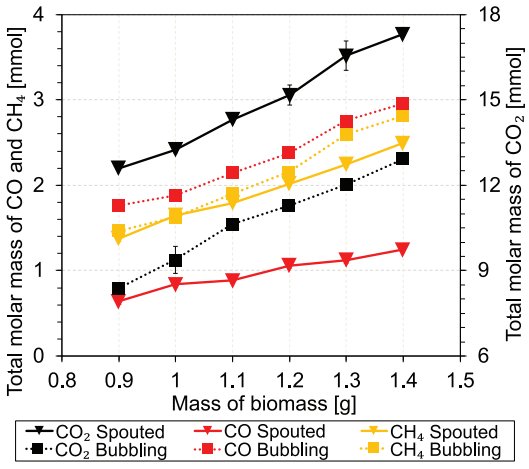

Fig. 11. Total detected amount of CH_4, CO and CO_2 during oxygen carrier aided devolatilization in relation to the amount of biomass used for the bubbling and spouted bed setup.

4.3.2. Gas species differences

In Fig. 11, the total detected amounts of a gas species in mmol are plotted against the amount of biomass used. Error bars are included for all data points. If the error bars are not visible, it is due to them being too small. Only a few data points exhibit visible error bars, and even in these cases, statistical significance remains evident, as the adjacent data points lie outside the range of these error bars.

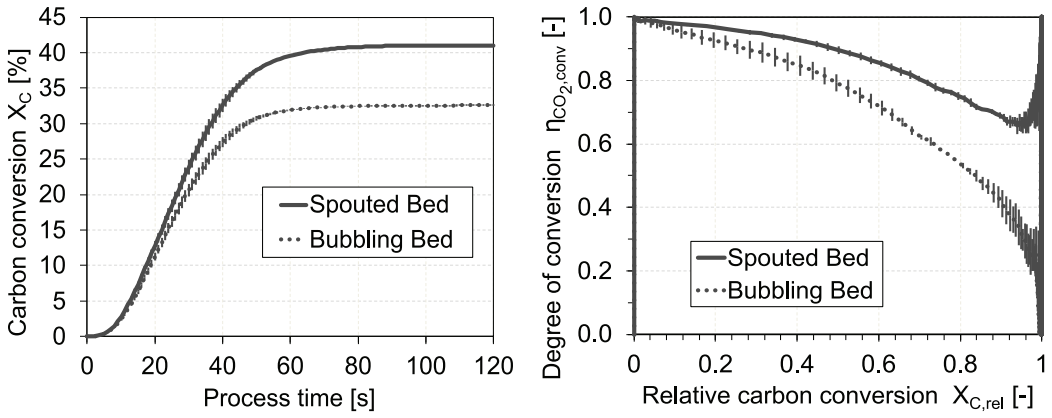

Fig. 12. Carbon conversion X_C plotted over time on the left and CO_2 specific degree of conversion $\eta_{CO_2,conv}$ plotted over relative carbon conversion $X_{C,rel}$ on the right. Both plots show average values from duplicate measurements for a biomass amount of 0.9 g for both the bubbling and spouted bed setup.

Both experimental setups, as expected, exhibited higher concentrations of carbonaceous gases with increasing fuel masses, which is due to higher total amounts of carbon being available for conversion. This increase in total molar masses is consistent with the increase of biomass. Notably, CO_2 amounts in the spouted bed were 33 to 50 % higher than in the bubbling bed setup. This difference can be attributed to longer contact times in the spouted bed, resulting from enhanced mixing, whereas volatiles in the bubbling bed had fewer opportunities to interact with the oxygen carrier. CO concentration measurements further support this observation, as they were decreased by between 64 and 57 % in the bubbling bed depending on the mass of biomass, indicating poorer gas-solid contact in the bubbling bed. Additionally, CH_4 concentrations increased with rising biomass mass in both setups; however, only smaller relative differences were observed between the two operation modes, with the spouted bed decreasing the total amount of methane produced between 0 and 14 %.

4.3.3. Conversion and degree of conversion

As shown in Fig. 12, left, both systems exhibit a steep increase in conversion up to approximately 45 s, after which the conversion curves flatten, reaching a maximum around 90 s.

The trends discussed above are also evident in Fig. 12, right. Since process times vary under different conditions, the CO_2-specific degree of conversion is plotted against relative carbon conversion rather than process time. This approach enables direct comparability between two different experimental runs.

These figures further illustrate that the spouted bed setup achieves higher total carbon conversions in a shorter time, leading to higher carbon conversion rates. However, the total conversion values remain below their theoretical maximum due to the limited amount of oxygen carrier (OC) material available for reaction, leading to sub-stoichiometric conditions.

The differences between the reactor types become particularly evident under these more demanding conditions. Even at the end of the conversion process, the spouted bed setup continues converting a significant fraction of the volatiles completely to CO_2, whereas in the bubbling bed, the degree of conversion declines sharply when relative carbon conversion approaches 0.7. This is due to the enhanced mixing in the spouted bed in combination with the floating of wood pellets on the bed surface in the fluidized bed and the resulting low contact time between gases and reactive bed material. Due to the better position of the pellet during devolatilization in the deeper bed zones in the spouted bed, the carbonaceous gases can still be converted in large parts to CO_2. The reason for this are higher residence times and enhanced contact between the oxygen carrier material and the gases.

4.3.4. Mass dependencies

Another way to compare the fluidization types is the carbon conversion. A value of 100 % cannot be achieved since fixed carbon is not converted during these conditions, because no gasification agent is present at high enough concentrations. Still, the difference is a reliable indicator to compare the fluidized bed setups. The superior performance of the spouted bed is reflected in consistently higher maximum carbon conversion for all investigated pellet masses as shown in Fig. 13, left. However, due to limitations in the amount of reactive bed material available, only a finite quantity of biomass can be converted. This could be a possible reasoning behind the decrease in total carbon conversion with increasing pellet mass in the spouted bed. If the total amount of convertible volatiles is reached in the spouted bed setup, this trend would not be due to reduced efficiency but rather to the fact that, while the absolute amount of converted biomass remains constant, its percentage relative to the total biomass input decreases.

Furthermore, the spouted bed exhibits a higher maximum carbon conversion rate regardless of the mass of biomass used, as shown in Fig. 13, right. Notably, the conversion rate remains unchanged with increasing mass of biomass, maintaining values of 0.97 %/s for the spouted bed and 0.83 %/s under bubbling bed conditions.

5. Conclusion

The findings of this study confirm that the use of a spouted bed configuration in chemical looping combustion (CLC) significantly improves the conversion of released volatiles during devolatilization of biomass fuels. The spouted bed enhances gas-solid contact and increases mechanical stress on fuel particles, leading to better mixing and fragmentation. The stability analysis demonstrated that the chosen operating conditions allowed for stable spouted bed operation at 800 °C. During combustion, higher carbon dioxide (CO_2) concentrations and reduced carbon monoxide (CO) emissions in the spouted bed indicated more complete conversion of volatiles. Additionally, at higher pellet masses, temporary oxygen depletion in case of the spouted bed setup was signaling faster devolatilization in case of the spouted bed setup. For oxygen carrier-aided devolatilization, the spouted bed setup exhibited longer process times caused by improved mixing and increased carbon conversion. CO_2 yields were 33–50 % higher than in the fluidized bed, confirming more efficient volatile conversion. Furthermore, the spouted bed reached higher maximum carbon conversion and also maintained higher carbon conversion rates across all biomass masses, reaching 0.97 %/s compared to 0.83 %/s in the fluidized bed. Overall, these results demonstrate that spouted beds enhance devolatilization of solid fuels in CLC conditions by improving fuel fragmentation, mixing, and gas-solid interactions. Future studies in this group will focus on the gasification part of CLC and whether spouted bed reactors can also improve reaction kinetics in this regard.

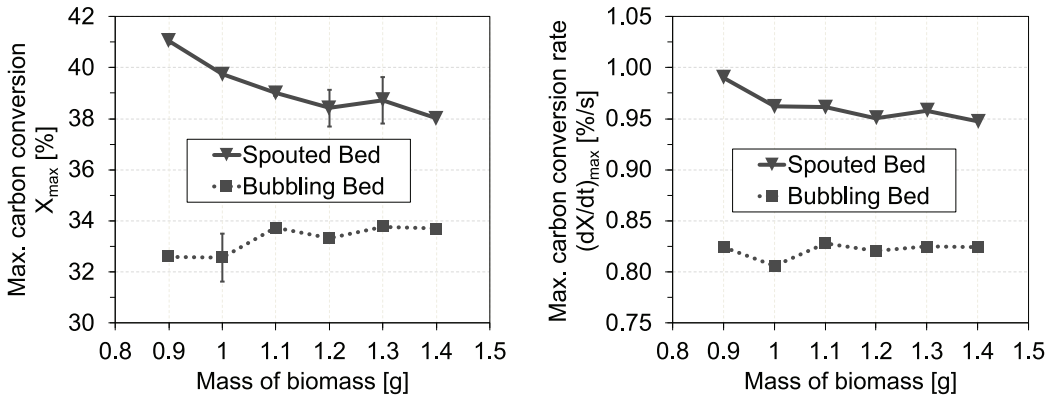

Fig. 13. Average maximum value of reached carbon conversion X_{max} depending on the mass of biomass used shown on the left. Average rate of carbon conversion $(dX/dt)_{max}$ depending on the mass of biomass used shown on the right.

CRediT authorship contribution statement

Marian Schmitt: Writing – review & editing, Writing – original draft, Visualization, Validation, Supervision, Software, Project administration, Methodology, Investigation, Formal analysis, Data curation, Conceptualization. **Lennard Lindmüller:** Writing – review & editing, Supervision, Project administration. **Alexander Fritzler:** Validation, Software, Methodology, Investigation, Formal analysis, Data curation, Conceptualization. **Stefan Heinrich:** Writing – review & editing, Supervision, Resources, Project administration, Funding acquisition.

Declaration of competing interest

The authors declare that they have no known competing financial interests or personal relationships that could have appeared to influence the work reported in this paper.

Acknowledgments

The financial support of the German Research Foundation DFG (Deutsche Forschungsgemeinschaft) under project number 495012431 is gratefully acknowledged.

Data availability

Data will be made available on request.

References

[1] M. Crippa, D. Guizzardi, E. Solazzo, M. Muntean, E. Schaaf, F. Monforti-Ferrario, M. Banja, J. Olivier, G. Grassi, S. Rossi, et al., GHG emissions of all world countries, Publ. Off. Eur. Union (2021).

[2] F.A. Rahman, M.M.A. Aziz, R. Saidur, W.A.W.A. Bakar, M. Hainin, R. Putrajaya, N.A. Hassan, Pollution to solution: Capture and sequestration of carbon dioxide (CO 2) and its utilization as a renewable energy source for a sustainable future, Renew. Sustain. Energy Rev. 71 (2017) 112–126, http://dx.doi.org/10.1016/j.rser.2017.01.011.

[3] C. Gough, P. Upham, Biomass energy with carbon capture and storage (BECCS or Bio-CCS), Greenh. Gases: Sci. Technol. 1 (4) (2011) 324–334.

[4] M. Shahbaz, A. AlNouss, I. Ghiat, G. Mckay, H. Mackey, S. Elkhalifa, T. Al-Ansari, A comprehensive review of biomass based thermochemical conversion technologies integrated with CO2 capture and utilisation within BECCS networks, Resour. Conserv. Recycl. 173 (2021) 105734.

[5] J. Adánez, A. Abad, T. Mendiara, P. Gayán, L. de Diego, F. García-Labiano, Chemical looping combustion of solid fuels, Prog. Energy Combust. Sci. 65 (2018) 6–66, http://dx.doi.org/10.1016/j.pecs.2017.07.005.

[6] J. Adánez, A. Abad, Chemical-looping combustion: Status and research needs, Proc. Combust. Inst. 37 (4) (2019) 4303–4317, http://dx.doi.org/10.1016/j.proci.2018.09.002.

[7] H. Gu, L. Shen, S. Zhang, M. Niu, R. Sun, S. Jiang, Enhanced fuel conversion by staging oxidization in a continuous chemical looping reactor based on iron ore oxygen carrier, Chem. Eng. J. 334 (2018) 829–836.

[8] P. Ohlemüller, J.-P. Busch, M. Reitz, J. Ströhle, B. Epple, Chemical-looping combustion of hard coal: autothermal operation of a 1 MWth pilot plant, J. Energy Resour. Technol. 138 (4) (2016) 042203.

[9] T. Mendiara, A. Pérez-Astray, M. Izquierdo, A. Abad, L. De Diego, F. García-Labiano, P. Gayán, J. Adánez, Chemical looping combustion of different types of biomass in a 0.5 kWth unit, Fuel 211 (2018) 868–875.

[10] C. Linderholm, A. Lyngfelt, A. Cuadrat, E. Jerndal, Chemical-looping combustion of solid fuels–Operation in a 10 kW unit with two fuels, above-bed and in-bed fuel feed and two oxygen carriers, manganese ore and ilmenite, Fuel 102 (2012) 808–822.

[11] A. Thon, M. Kramp, E.-U. Hartge, S. Heinrich, J. Werther, Operational experience with a system of coupled fluidized beds for chemical looping combustion of solid fuels using ilmenite as oxygen carrier, Appl. Energy 118 (2014) 309–317, http://dx.doi.org/10.1016/j.apenergy.2013.11.023.

[12] J. Haus, L. Lindmüller, T. Dymala, K. Jarolin, Y. Feng, E.-U. Hartge, S. Heinrich, J. Werther, Increasing the efficiency of chemical looping combustion of biomass by a dual-stage fuel reactor design to reduce carbon capture costs, Mitig. Adapt. Strat. Glob. Chang. 25 (2020) 969–986.

[13] L. Lindmüller, J. Haus, S. Heinrich, High volatile conversion in a chemical looping combustion system with three different biomasses, Energy Fuels 36 (17) (2022) 9529–9537, http://dx.doi.org/10.1021/acs.energyfuels.2c00901.

[14] L. Lindmüller, J. Haus, A.R.K. Nair, S. Heinrich, Minimizing gas leakages in a system of coupled fluidized bed reactors for chemical looping combustion, Chem. Eng. Sci. 250 (2022) 117366.

[15] K.B. Mathur, P.E. Gishler, A technique for contacting gases with coarse solid particles, AIChE J. 1 (2) (1955) 157–164, http://dx.doi.org/10.1002/aic.690010205.

[16] C.J. Lim, A.P. Watkinson, G.K. Khoe, S. Low, N. Epstein, J.R. Grace, Spouted, fluidized and spout-fluid bed combustion of bituminous coals, Fuel 67 (9) (1988) 1211–1217.

[17] M.G. Rasul, Spouted bed combustion of wood charcoal: performance comparison of three different designs, Fuel 80 (15) (2001) 2189–2191.

[18] P.A. Salam, S. Bhattacharya, A comparative study of charcoal gasification in two types of spouted bed reactors, Energy 31 (2–3) (2006) 228–243.

[19] A.P. Watkinson, A.C. Lisboa, 15 Gasification, pyrolysis, and combustion, Spouted Spout- Fluid Beds: Fundam. Appl. (2010) 250.

[20] R. Boerefijn, M. Ghadiri, P. Salatino, Attrition in fluidised beds, Handb. Powder Technol. 12 (2007) 1019–1053.

[21] K. Mather, Spouted Beds, Elsevier, 2012.

[22] A.R. Fernández-Akarregui, J. Makibar, I. Alava, L. Diaz, F. Cueva, R. Aguado, G. Lopez, M. Olazar, Sand attrition in conical spouted beds, Particuology 10 (5) (2012) 592–599.

[23] J. Haus, M. Goltzsche, E.-U. Hartge, S. Heinrich, J. Werther, Gasification kinetics of lignite char in a fluidized bed of reactive oxygen carrier particles, Fuel 236 (2019) 166–178, http://dx.doi.org/10.1016/j.fuel.2018.08.151.

[24] M. Olazar, M.J. San Jose, A.T. Aguayo, J.M. Arandes, J. Bilbao, Stable operation conditions for gas-solid contact regimes in conical spouted beds, Ind. Eng. Chem. Res. 31 (7) (1992) 1784–1792.

[25] M. Olazar, M.J. San José, S. Alvarez, A. Morales, J. Bilbao, Design of conical spouted beds for the handling of low-density solids, Ind. Eng. Chem. Res. 43 (2) (2004) 655–661.

[26] N. Epstein, J.R. Grace, Spouted and Spout-Fluid Beds: Fundamentals and Applications, Cambridge University Press, 2010.

[27] DIN 51718:2002-06, Prüfung fester Brennstoffe_- Bestimmung des Wassergehaltes und der Analysenfeuchtigkeit, Tech. Rep., Beuth Verlag GmbH, http://dx.doi.org/10.31030/9226705.

[28] DIN 51719:1997-07, Prüfung fester Brennstoffe_- Bestimmung des Aschegehaltes, http://dx.doi.org/10.31030/7346447.

[29] DIN 51720:2001-03, Prüfung fester Brennstoffe_- Bestimmung des Gehaltes an Flüchtigen Bestandteilen, http://dx.doi.org/10.31030/9065360.
[30] A. Sadeq, D. Heinrich, S. Pietsch-Braune, S. Heinrich, Influence of oscillating water content on the structure of biomass pellets, Powder Technol. 426 (2023) 118631, http://dx.doi.org/10.1016/j.powtec.2023.118631.
[31] L.F. De Diego, P. Gayán, F. García-Labiano, J. Celaya, A. Abad, J. Adánez, Impregnated CuO/Al2O3 oxygen carriers for chemical-looping combustion: avoiding fluidized bed agglomeration, Energy Fuels 19 (5) (2005) 1850–1856.
[32] P. Bolt, F.H. Habraken, J. Geus, Formation of nickel, cobalt, copper, and iron aluminates fromα-andγ-alumina-supported oxides: a comparative study, J. Solid State Chem. 135 (1) (1998) 59–69.
[33] N. Mostoufi, G. Kulah, M. Koksal, Flow structure characterization in conical spouted beds using pressure fluctuation signals, Powder Technol. 269 (2015) 392–400, http://dx.doi.org/10.1016/j.powtec.2014.09.028.
[34] M. Mayerhofer, S. Fendt, H. Spliethoff, M. Gaderer, Fluidized bed gasification of biomass–In bed investigation of gas and tar formation, Fuel 117 (2014) 1248–1255.
[35] A. Pérez-Astray, I. Adánez-Rubio, T. Mendiara, M. Izquierdo, A. Abad, P. Gayán, L. de Diego, F. García-Labiano, J. Adánez, Comparative study of fuel-N and tar evolution in chemical looping combustion of biomass under both iG-CLC and CLOU modes, Fuel 236 (2019) 598–607.
[36] N.M. Nguyen, F. Alobaid, P. Dieringer, B. Epple, Biomass-based chemical looping gasification: Overview and recent developments, Appl. Sci. 11 (15) (2021) 7069.
[37] D. Pallares, F. Johnsson, Modeling of fuel mixing in fluidized bed combustors, Chem. Eng. Sci. 63 (23) (2008) 5663–5671.
[38] P. Salatino, P. Ammendola, P. Bareschino, R. Chirone, R. Solimene, Improving the thermal performance of fluidized beds for concentrated solar power and thermal energy storage, Powder Technol. 290 (2016) 97–101.